Uncertainties of mass extrapolations in Hartree-Fock-Bogoliubov mass models

S. Goriely[1] and R. Capote[2]

[1]*Institut d'Astronomie et d'Astrophysique, Université Libre de Bruxelles, CP 226, B-1050 Brussels, Belgium*

[2]*NAPC–Nuclear Data Section, International Atomic Energy Agency, Vienna International Centre, Vienna A-1400, Austria*

(Received 4 March 2014; revised manuscript received 22 April 2014; published 23 May 2014)

Some 27 Hartree-Fock-Bogoliubov (HFB) mass models have been developed by the Brussels-Montreal collaboration. Each of these models has been obtained with different model prescriptions or corresponds to a significantly different minimum in the parameter space. The corresponding uncertainties in the mass extrapolation are discussed. In addition, for each of these models, uncertainties associated with local variations of the model parameters exist. Those are estimated for the HFB-24 mass model using a variant of the backward-forward Monte Carlo method to propagate the uncertainties on the masses of exotic nuclei far away from the experimentally known regions. The resulting uncertainties are found to be significantly lower than those arising from the 27 HFB mass models. In addition, the derived correlations between the calculated masses and between model parameters are analyzed.

DOI: 10.1103/PhysRevC.89.054318 PACS number(s): 21.10.Dr, 21.60.−n, 21.65.Mn, 26.30.−k

I. INTRODUCTION

The nuclear energy density functional theory has been very successful in describing the properties and the dynamics of a wide range of nuclei [1]. Among the most popular functionals are those obtained from zero-range effective interactions of the Skyrme type, which allow fast numerical computations in the framework of the self-consistent Hartree-Fock-Bogoliubov (HFB) method. The parameters of these interactions are determined so as to reproduce a set of nuclear data selected according to a specific purpose. The nonuniqueness of the fitting procedure has thus led to a large number of different parametrizations. Some of them may yield very different predictions when applied outside the domain where they were fitted [2].

This situation is particularly unsatisfactory for nuclear astrophysical applications, which require the knowledge of nuclear masses for nuclei so neutron rich that there is no hope of measuring them in the foreseeable future; such nuclei play a vital role in the r-process of nucleosynthesis [3] and are also found in the outer crust of neutron stars [4]. Extrapolations far beyond the neutron drip line are required for the description of the inner crust of neutron stars where at high densities neutron-proton clusters coexist with free neutrons in Wigner-Seitz-type cells [5]. The need for more reliable extrapolations of these nuclear models has motivated recent efforts to construct mass models within the Skyrme-HFB framework that can compete with the most sophisticated microscopic-macroscopic mass models. Those Skyrme functionals are adjusted to reproduce, in addition to the properties of finite nuclei, the predictions in infinite homogeneous nuclear matter (INM), in particular pure neutron matter, as given by realistic calculations.

During the past decade there has been a considerable increase in the demand for nuclear data that provide some specification of the estimated uncertainties in the results [6]. New stochastic methods have been developed to estimate uncertainties from theoretical calculations including both parameter [7] and model uncertainties [8]. Monte Carlo (MC) methods (e.g., see Ref. [6]) allow to combine model calculations with the available experimental data to reduce the uncertainties of the evaluated data [9–11]. Modern nuclear system analysis procedures are now able to accommodate nuclear data uncertainties, thereby providing further stimulus for their estimation. Although sensitivity analyses have been performed in the framework of mass models [12,13], no uncertainty propagation to experimentally unknown masses has been performed. It remains therefore unknown how accurate a model prediction can be when extrapolated to exotic nuclei, as those involved in nuclear applications like nucleosynthesis. The goal of the present paper is to apply modern evaluation techniques to assess the uncertainties on HFB-predicted nuclear masses that are needed in many nuclear applications (e.g., nuclear power applications and astrophysics), but which cannot be measured. In Sec. II, the Brussels-Montreal HFB mass models are described and the 1σ uncertainties between the 27 mass tables estimated for the 8500 nuclei included in these tables. In Sec. III, the uncertainties associated with local variations of the model parameters around the HFB-24 minimum are calculated on the basis of an MC uncertainty propagation. The corresponding analysis provides in Sec. IV a study of the various correlations inherent to the model as well as those existing between the model parameters.

II. HFB MASS MODELS

Since the publication of the first HFB mass model [14], another 26 HFB mass models have been developed and published [15–28]. While the first HFB-1 mass model [14] aimed at proving that is was possible to reach a low root-mean-square (rms) deviation with respect to all experimental masses available at that time, most of the subsequent models were developed to further explore the parameter space widely or to take into account additional constraints. In this way, the interaction was refitted either to consider new experimental mass data [15,27] or to improve the description of empirical fission barriers [21] or to study the sensitivity of the mass model accuracy and extrapolation to major changes in the description of the pairing interaction [16,20,23] or of the

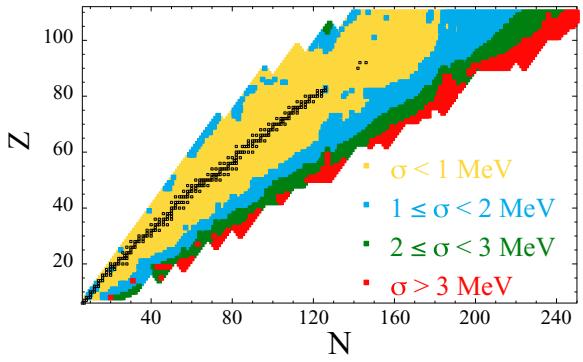

FIG. 1. (Color online) 1σ uncertainty corresponding to the 27 HFB mass models for all the 8500 nuclei included in the mass tables from $Z = 8$ up to $Z = 110$.

nuclear matter properties, such as the effective mass [17], the symmetry energy [19,26,27], and the stability of the equation of state [23,26]. Some model uncertainties, in particular in the treatment of number projection [18] or Coulomb correlations [22] were also studied. Two breakthroughs were achieved when improvements in the parameter adjustments allow us to reach the subjective 0.6 [24] and 0.5 MeV [28] thresholds in the model rms deviation.

With respect to the 2353 measured masses [29], the 27 HFB mass models present rms deviations between 0.51 MeV for HFB-27 [28] and 0.79 MeV for HFB-1 [14]. However, when dealing with exotic nuclei far away from stability, deviations between the HFB mass predictions can become significant, not only in the rigidity of the mass parabola, but also in the description of the shell gaps or pairing correlations. The 1σ variance between the 27 HFB mass predictions are illustrated in Fig. 1 where deviations larger than 3 MeV can be found at the neutron drip lines. Such large uncertainties can be interpreted as our model uncertainties (due to model defects) [8] and are considered to be independent of parameter uncertainties, but rather a property of the given HFB model.

To estimate the model parameter uncertainties and the corresponding uncertainties in the mass predictions associated with each of these mass models, we consider the functional BSk24 and corresponding mass model HFB-24 [27]. Though all details about the HFB calculation and the elaboration of the HFB-24 mass model can be found in Ref. [27], we recall here some of the important features. The BSk24 functional is based on an effective force with the 16-parameter generalized Skyrme form

$$
\begin{aligned}
v_{ij} &= t_0(1+x_0P_\sigma)\delta(\boldsymbol{r}_{ij}) \\
&+ \frac{1}{2}t_1(1+x_1P_\sigma)\frac{1}{\hbar^2}\left[p_{ij}^2\,\delta(\boldsymbol{r}_{ij}) + \delta(\boldsymbol{r}_{ij})\,p_{ij}^2\right] \\
&+ t_2(1+x_2P_\sigma)\frac{1}{\hbar^2}\boldsymbol{p}_{ij}\cdot\delta(\boldsymbol{r}_{ij})\,\boldsymbol{p}_{ij} \\
&+ \frac{1}{6}t_3(1+x_3P_\sigma)\,n(\boldsymbol{r})^\alpha\,\delta(\boldsymbol{r}_{ij}) \\
&+ \frac{1}{2}t_4(1+x_4P_\sigma)\frac{1}{\hbar^2}\left[p_{ij}^2\,n(\boldsymbol{r})^\beta\,\delta(\boldsymbol{r}_{ij}) + \delta(\boldsymbol{r}_{ij})\,n(\boldsymbol{r})^\beta\,p_{ij}^2\right] \\
&+ t_5(1+x_5P_\sigma)\frac{1}{\hbar^2}\boldsymbol{p}_{ij}\cdot\,n(\boldsymbol{r})^\gamma\,\delta(\boldsymbol{r}_{ij})\,\boldsymbol{p}_{ij} \\
&+ \frac{\mathrm{i}}{\hbar^2}W_0(\boldsymbol{\sigma_i}+\boldsymbol{\sigma_j})\cdot\boldsymbol{p}_{ij}\times\delta(\boldsymbol{r}_{ij})\,\boldsymbol{p}_{ij}, \qquad (1)
\end{aligned}
$$

where $\boldsymbol{r}_{ij} = \boldsymbol{r}_i - \boldsymbol{r}_j, \boldsymbol{r} = (\boldsymbol{r}_i + \boldsymbol{r}_j)/2$, $\boldsymbol{p}_{ij} = -\mathrm{i}\hbar(\boldsymbol{\nabla}_i - \boldsymbol{\nabla}_j)/2$ (this is the relative momentum), P_σ is the two-body spin-exchange operator, and $n(\boldsymbol{r}) = n_n(\boldsymbol{r}) + n_p(\boldsymbol{r})$ is the total local density, with $n_n(\boldsymbol{r})$ and $n_p(\boldsymbol{r})$ being the neutron and proton densities, respectively. The t_4 and t_5 terms are unconventional, being density-dependent generalizations of the t_1 and t_2 terms, respectively. The full formalism for this generalized Skyrme force is presented in the Appendix of Ref. [25], but note that all the terms in J^2 and J_q^2 are dropped from the Hamiltonian density, as discussed in Ref. [26].

The pairing force has a δ-function form

$$
v_q^{\mathrm{pair}}(\boldsymbol{r_i},\boldsymbol{r_j}) = f_q^\pi\,v[\rho_n(\boldsymbol{r}),\rho_p(\boldsymbol{r})]\delta(\boldsymbol{r}_{ij}), \qquad (2)
$$

where $v[\rho_n,\rho_p]$ is a functional of both the neutron and proton densities, calculated analytically at each point in the nucleus in question in such a way as to reproduce the $^1S_0$ pairing gaps of INM at the appropriate density and charge asymmetry, as determined by many-body calculations with realistic two- and three-nucleon forces [23,24]. The INM constraint determines the strength of the pairing force almost completely, but we introduce some fine-tuning of the strengths in the form of the four global renormalization parameters f_q^π, which allow the overall strength to be slightly different for neutrons than for protons, and which also permit each of these strengths to depend on whether there is an even or odd number of nucleons of the charge type in question. In this way we take into account Coulomb effects as well as the slight violation of time reversibility implicit in our treatment of odd nuclei. A cutoff parameter ε_Λ to the single-particle spectrum is introduced, as described in Ref. [23].

Finally, the total energy is deduced from the HFB energy by subtracting an estimate for the spurious collective energy based on the cranking approximation [21], and a phenomenological Wigner correction energy [15] which contributes significantly only for light nuclei or nuclei with N close to Z.

BSk24 has been shown to reproduce the 2353 measured masses of nuclei with N and $Z \geqslant 8$ appearing in the 2012 Atomic Mass Evaluation [29] with an rms deviation of 0.549 MeV. In making the parameter adjustment, the Skyrme part of the functional was simultaneously constrained to fit the stiff zero-temperature equation of state of homogeneous neutron matter, as determined by many-body calculations with realistic two- and three-nucleon forces [30] to support the more massive observed neutron stars. In addition, BSk24 was also constrained to reproduce several other properties of INM as obtained from many-body calculations. Among those, (i) the ratio of the isoscalar effective mass m_s^* to bare nucleon mass m in symmetric INM at saturation was set to the realistic value of 0.8; (ii) a neutron effective mass that is larger than the proton effective mass in neutron-rich matter, as found both experimentally and from microscopic calculations; (iii) the incompressibility of symmetric INM at saturation K (which was required to fall in the experimental range 240 ± 10 MeV, according to the authors of Ref. [31]); (iv) supports the heaviest

observed neutron stars. Finally, all unphysical instabilities of nuclear matter, including the transition to a polarized state in neutron-star matter, are eliminated with BSk24.

III. MODEL PARAMETER UNCERTAINTIES

In HFB-24, all together, there are 30 model parameters, namely 16 Skyrme parameters, 5 pairing parameters, 4 Wigner parameters, and 5 collective parameters. Each parameter has been adjusted to optimize the prediction of the 2353 experimental masses of nuclei with N and $Z \geqslant 8$ appearing in the 2012 Atomic Mass Evaluation [29], leading to an rms deviation $\sigma_{\rm exp} = 0.549$ MeV. However, each of the 30 parameters is affected by some uncertainty that could propagate and modify in particular the mass extrapolations of particular interest in nuclear applications. It is possible to estimate the impact of such model-parameter uncertainties on calculated masses by propagating the parameter uncertainties by Monte Carlo sampling constrained by available experimental masses [29]. The method considered here is similar to the backward-forward Monte Carlo (BFMC) method [32–34]. It relies on the sampling of model parameters and on the use of a generalized χ^2 estimator to quantify the likelihood of each model calculation result respective to a given set of experimental constraints on calculated masses. At this stage the correlation between model parameters appear. We avoided a resampling from the derived distribution of the parameters as proposed in the original BFMC method. Instead, we used the backward MC only for the selection of the suitable samples that agree with experimental constraints. Then, we used this selected set of the MC sample to calculate masses of nuclei not measured in the forward MC step. Finally, the mean values, uncertainties, and correlations on extrapolated masses were derived from the sampled population.

The adopted BFMC method consists of the following steps.

(i) Assessing the allowed range of variation in the vicinity of the local minimum for each of the model parameters.
(ii) Sampling model-parameter sets using assessed parameter uncertainties and assuming that model parameters are independent.
(iii) (Backward MC step [33,34]): Selecting those parameter sets from the sampled population using different weighting factors that depend on available experimental data.
(iv) (Forward MC step [33,34]): Using selected sampled parameter sets to additionally calculate experimentally unknown masses (without resampling from derived parameter distributions).
(v) Deriving the first and second moments (the mean value and covariance) of the estimated observables (nuclear masses) from the sample obtained for all nuclei in step 4.

It should be remarked that the method proposed above does not require to derive model-parameter uncertainties and covariances at the backward MC step (even if we can do that to study the statistical distribution of those quantities). Instead, the full sampled parameter sets are used. This avoids the approximation of neglecting the third and higher moments of the model-parameter distribution.

In the BFMC method introduced in Refs. [32–34], the χ^2 estimator is used to estimate a likelihood function that will weight the $\{p_1, \ldots, p_n\}$ sample more when the associated observables $\{M_1, \ldots, M_m\}$ are close to the experimental data. More specifically, the suggested weighting function is

$$w_i = C \exp\left(- \left(\chi_i^2/\chi_{\rm min}^2\right)^2\right), \tag{3}$$

where $\chi_{\rm min}^2$ represents the minimal value of the χ^2 function, i.e., the reference HFB-24 χ^2 in our case. C is a normalizing constant that is not relevant for mean value and covariance calculations as it cancels out. The tabulation of experimental masses does not contain estimates of experimental correlations between measured masses, although such correlations may exist. In this work we assume that all experimental measured mass values are independent, which may reduce our assessed uncertainty. However, our focus is to study the uncertainties of predicted masses, where no experimental data are available. This assumption allows us to use a simple χ^2 criteria instead of the generalized one. In addition to this weighting function, we also consider here the threshold function

$$\begin{aligned} w_i = 1 \quad &\text{for} \quad \chi_i \leqslant \chi_{\rm crit}, \\ 0 \quad &\text{for} \quad \chi_i > \chi_{\rm crit}, \end{aligned} \tag{4}$$

where $\chi_{\rm crit}$ is a critical value. Note that both functions are biased towards model predictions rather than experimental data [9–11]. An unbiased weighting function was proposed in the unified Monte Carlo approach (UMC-B [35])

$$w_i = C \exp\left(- \chi_i^2\right). \tag{5}$$

The main difference to Eq. (3) is the lack of the renormalization factor $\chi_{\rm min}^2$. However, the UMC-B method would require an even larger numerical effort than with the above-mentioned weighting functions given by Eqs. (3) and (4). The reason is that the absolute χ_i^2 value tends to be larger than the normalized quantity $\chi_i^2/\chi_{\rm min}^2$, so the weight calculated by Eq. (5) is smaller in the UMC-B. Therefore, a much larger set of sampled parameters is required to achieve convergence of the mean value and covariance calculations.

Unfortunately, HFB calculations remain very time consuming due to the large number of experimental data (2353 masses) on one side and exotic nuclei of interest in nuclear astrophysics applications (typically some 8000 nuclei), therefore some simplifying strategies need to be adopted, even within the BFMC method. Applications of UMC-B would require massive parallel calculations. In this work, we made the following simplifying assumptions.

(i) All sensitivity calculations of the model parameters are performed assuming nuclei are spherical. All calculations assume that the deformation energy (i.e., the difference between the energy in the spherical configuration and the potentially deformed ground-state energy) remains unaffected by the small parameter variations.
(ii) Only the 21 parameters corresponding to the generalized Skyrme and pairing interactions are varied

since varying the five collective parameters would imply breaking the spherical symmetry and the Wigner parameters have a restricted impact on light or $Z \simeq N$ nuclei only. In addition, the 21 parameters are assumed to be independent.

(iii) The major experimental constraint stemming from measured masses is reduced to a sample of 729 nuclei, i.e., a third of the $|N - Z| > 2$ measured masses [29], as used in the fitting procedure explained in Ref. [27].

(iv) The study of mass uncertainties of experimentally unknown nuclei is restricted to the 1707 even-even nuclei with $8 \leqslant Z \leqslant 110$ and lying between the proton and neutron drip lines.

Finally, as the χ^2 estimator, we consider here the mean square deviation $\sigma^2_{\rm exp}$ with respect to the 729 nuclei used in our sample of experimental masses. This choice is consistent with the quantitative criterion used to adjust the HFB parameters [27]. Since all the 27 HFB mass models are characterized with an rms deviation smaller than typically 0.8 MeV, a natural choice of the the critical value entering Eq. (4) would be to take the same value. To test the sensitivity of our results with respect to the adopted weighting function, we also consider in the present work the two values of 0.6 and 1 MeV, as well as the original weighting function [Eq. (3)] introduced in the BFMC method [32–34]. Future analysis along the UMC-B approach will be reported in a forthcoming work. Each of the BFMC steps are now detailed in the next sections.

A. Assessing HFB parameter uncertainties

To estimate the uncertainty affecting our 21 model parameters, we use the rms deviation with respect to the 729 experimental masses. Each of the 21 parameters p defining the Skyrme and pairing interactions have been varied and given a relative uncertainty $\Delta p/p$ such that an individual change of each parameter leads to a maximum 10% increase of the rms deviation with respect to the 729 experimental masses in our sample. Our local HFB-24 minimum gives rise to an rms deviation of 0.510 MeV ($=\chi^2_{\rm min}$) with respect to the 729 masses. The relative uncertainty for each of the 21 parameters therefore corresponds to an individual parameter change leading to an rms deviation of the order of 0.560 MeV. Note that the 10% increase of the rms deviation is chosen to optimize the sampling needed to get a significant statistics in the BFMC method (see below), but is not expected to affect the results. Indeed, a larger value would essentially request more cases to be calculated to achieve a similar significant sample of runs constrained by the χ^2 estimator on experimental data [as given by Eqs. (3) and (4)].

The associated relative uncertainties for each parameter are shown in Fig. 2 and are seen to be rather small for the adopted criterion of a 10% increase of the rms deviation (the largest uncertainty of 9% is found for the x_1 parameter, which consequently needs to be significantly modified to affect the masses). Obviously a systematic modification of all the parameters would lead to a larger increase of the rms deviation, as will be shown in Sec. IIIB. However, on the basis of Fig. 2, it is believed that the deformation energy as well as the collective and Wigner correction energies are not significantly affected by such local variations; this justifies the simplifying assumptions made that the parameter uncertainties can be essentially estimated in the spherical approximation. Since the 21 parameters are assumed to be independent, the associated parameter covariance matrix is the unit matrix. It should be noted that the assumption that parameters are uncorrelated will be invalidated as soon as we consider experimental constraints, as will be shown in the next section.

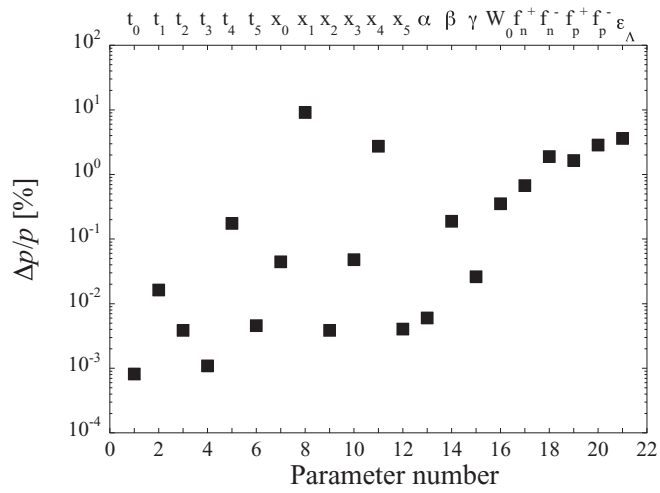

FIG. 2. Assumed relative uncertainties on each of the 21 model parameters of the BSk24 functional. The relative parameter uncertainty is defined as the relative change leading to an increase of the rms deviation by 10%. The parameter labeling is shown on the upper x axis.

Each of the 21 model parameters with their relative uncertainty $\Delta p/p$ is assumed to be normally distributed with the mean value $\langle p \rangle$ equal to the BSk24 value. Such an assumption is justified by the small parameter uncertainties shown in Fig. 2. Based on such a multidimensional probability density function, 29 300 spherical HFB calculations with randomly chosen sets of the 21 parameters are performed to obtain the full sample population.

B. Backward Monte Carlo step

The rms deviation with respect to the 729 experimental masses of our sample is used as the χ^2 estimator of the backward Monte Carlo step (point 3 above). The resulting distribution of rms deviations $\sigma_{\rm exp}$ on the 729 experimental masses is illustrated in Fig. 3. While only 1768 runs have an rms deviation $\sigma_{\rm exp} < 0.6$ MeV, rms deviations up to 4.0 MeV are found in the full sample set. From the obtained 29 300 samples of model parameter sets it is possible to derive (using the weighted formulas) the first (mean value $\langle p \rangle$) and second moments (covariances $\langle \Delta p_i \Delta p_j \rangle$) of the sampled parameter distribution.

Randomly sampled parameter sets are also used to calculate the masses of those nuclei having experimental information and the main nuclear matter properties, i.e., the Fermi momentum k_F and the incompressibility K of charge-symmetric INM, the symmetry coefficient J, the slope L of the symmetry

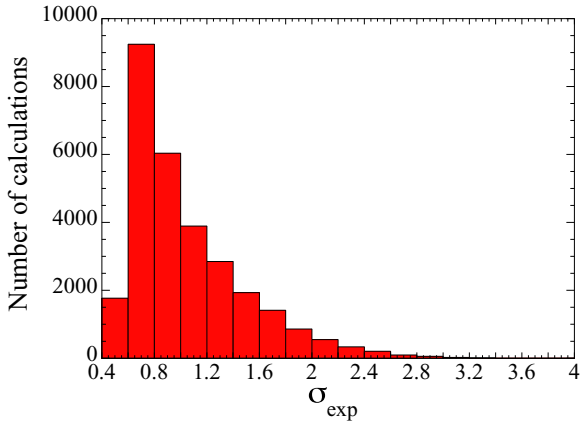

FIG. 3. (Color online) Distribution of rms deviations with respect to the 729 experimental masses [29] for the 29 300 MC calculations. The distributions are binned in steps of 0.2 MeV.

energy at the saturation density, and the isoscalar (m_s^*/m) and isovector (m_v^*/m) effective nucleon masses. From those random samples it is also possible to derive the first (e.g., the mean nuclear mass $\langle M \rangle$) and second momenta (e.g., mass covariance $\langle \Delta M_i \Delta M_j \rangle$) of the calculated masses and nuclear matter properties. The diagonal elements $\langle \Delta M_i \rangle^2$ of the derived covariance matrix corresponds to the square of the absolute uncertainty ΔM_i of the nuclear mass (or nuclear matter property). Derived mean values of the nuclear matter properties are given in Table I. The mean values are seen to be almost identical to the initial BSk24 values and the relative uncertainties remain rather small, as follows from the small variation allowed around the local BSk24 minimum (Fig. 2).

We also compared derived the mean value of nuclear masses $\langle M \rangle$ with the reference calculation $M_{\rm ref}$ that uses the mean value of the parameters $\langle p \rangle$ (without sampling). The differences between the mean mass values derived from the full sample with the reference calculation are found to be much smaller than the estimated mass uncertainty. This allows us to estimate the model nonlinearity and safely assume that estimated mass uncertainties can be used for the reference HFB-24 model without introducing an additional uncertainty.

C. Forward Monte Carlo step

The forward step of the BFMC method considers a given distribution of model parameters (represented by selected samples) that represents both the response of the model to parameter variations, and the experimental data that were used to constrain the distribution of model parameters. Out of the 29 300 calculations performed in Sec. III B, most of the runs can be qualified as giving rise to rather large deviations with respect to the bulk of measured masses, the rms deviation reaching values up to 4.0 MeV. However, 1768 runs have an rms deviation $\sigma_{\rm exp} \leqslant 0.6$ MeV, 11 013 predict measured masses with $\sigma_{\rm exp} \leqslant 0.8$ MeV, and 17 059 with $\sigma_{\rm exp} \leqslant 1.0$ MeV. Applying the weighting functions given in Eqs. (3) and (4), the 1σ uncertainty can be estimated on the masses of all the 1707 even-even nuclei with $8 \leqslant Z \leqslant 110$ and lying between the proton and neutron drip lines. The results are illustrated in Fig. 4. Uncertainties smaller than typically 2 MeV are found, only values up to 3 MeV can be reached for heavy nuclei at the neutron drip line. The resulting uncertainties are obviously greatest for the largest sample with $\sigma_{\rm exp} \leqslant$ 1.0 MeV [weighting function given by Eq. (4)], while the original BFMC method with the weighted function given by Eq. (3) provides uncertainties smaller than 2 MeV (lowest panel in Fig. 4). For all the cases considered here, comparing Figs. 1 and 4 clearly shows that the uncertainties associated with local changes of the HFB parameters remain significantly smaller than those associated with nonlocal changes as described by the 27 HFB mass models. The large degrees of freedom offered by the latter approach also allow for significantly different predictions of shell effects, pairing energies, deformation transitions, while the present analysis restricts the changes in the vicinity of the local minimum and consequently does not give rise to major changes, as is also seen for the derived INM mean properties given in Table I.

IV. MODEL AND PARAMETER CORRELATIONS

The BFMC analysis allows us to study the various correlations inherent to the model as well as those existing between the parameters used to describe the underlying physics. This represents a significant advantage for model developers by reducing the parameter space. Many of those correlations have already been studied earlier on grounds of algebraic relations or covariance analysis [12,13,36]. Three different kinds of

TABLE I. Mean $\langle p_d \rangle$, absolute Δp_d, and relative $\Delta p_d/p_d$ uncertainties on the nuclear matter properties derived from the HFB parameters. The first column corresponds to BSk24 values, the next three columns to mean value, absolute, and relative uncertainties from the 29 300 unconstrained Monte Carlo calculations and the next three columns to the 11 013 subset of runs with an rms deviation $\sigma_{\rm exp} < 0.8$ MeV (with respect to the 729 measured masses).

	BSk24	$\langle p_d \rangle$	Δp_d	$\Delta p_d/p_d$[%]	$\langle p_d \rangle$	Δp_d	$\Delta p_d/p_d$ [%]
k_F [fm^{-1}]	1.3270	1.3270	1.8×10^{-4}	0.014	1.3270	1.2×10^{-4}	0.009
a_v [MeV]	−16.048	−16.048	7.1×10^{-3}	0.044	−16.048	4.6×10^{-3}	0.029
J [MeV]	30.000	30.000	1.4×10^{-1}	0.454	30.001	1.2×10^{-1}	0.384
K [MeV]	245.523	245.524	1.0×10^{-1}	0.042	245.522	6.7×10^{-2}	0.027
L [MeV]	46.523	46.402	6.6×10^{-1}	1.432	46.395	5.7×10^{-1}	1.236
m_s^*/m	0.800	0.800	8.5×10^{-5}	0.011	0.800	7.5×10^{-5}	0.009
m_v^*/m	0.713	0.713	1.4×10^{-3}	0.202	0.713	1.3×10^{-3}	0.189

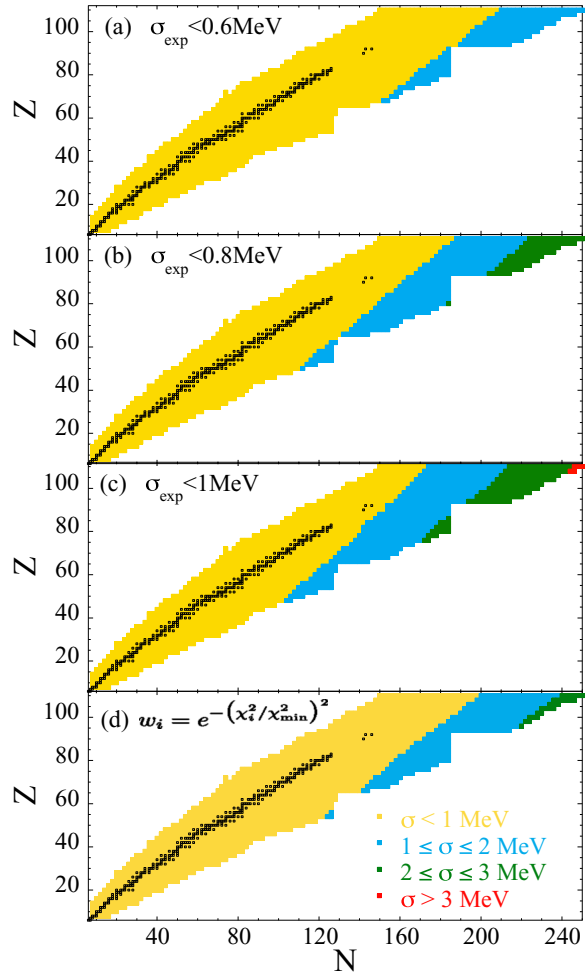

FIG. 4. (Color online) 1σ uncertainty for all even-even nuclei from $Z = 8$ up to $Z = 110$ lying between the proton and neutron drip lines and corresponding to (a) the 1768 runs with $\sigma_{exp} < 0.6$ MeV, (b) the 11 013 runs with $\sigma_{exp} < 0.8$ MeV, (c) the 17 059 runs with $\sigma_{exp} \leqslant 1.0$ MeV, or (d) all the runs with the weighted function given by Eq. (3).

covariance analysis are described in the next sections. It is worth noting that it is also possible to undertake evaluations in the observable (mass) space as done in UMC-B methods [9–11]. Such a choice would minimize the impact of model nonlinearities on our uncertainty quantification at the price of losing the ability to derive parameter correlations, and therefore to potentially improve the modeling.

A. Mass correlations

The BFMC method used here allows us to build the full covariance matrix for the calculated masses. It is illustrated in Fig. 5 for a sample of 105 masses out of the 729 considered in our sample of experimental masses. This sample covers the lightest ($Z = 8$) to the heaviest nuclei ($Z = 110$) with an equidistant step in mass number (step = 7 amu). Of particular interest is the observation that strong correlations (typically larger than 0.4) exist between the masses all over the full (N, Z) plane. Such strong correlations are typical

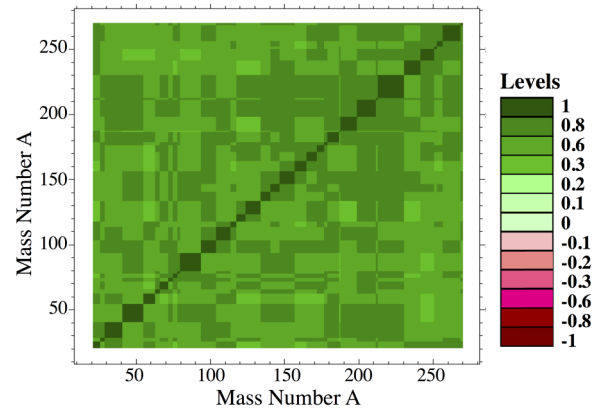

FIG. 5. (Color online) Color plot of the mass correlations $\langle \Delta p_i \Delta p_j \rangle$ estimated on the basis of the backward MC step. Correlations are calculated for a sample of 105 out of the 729 masses from our experimental masses covering the lightest ($Z = 8$) to the heaviest nuclei ($Z = 110$) with equidistant step in mass number.

of models, they reflect the fact that we use a very small number of parameters to describe a much larger set of observables. We expect models to be strongly correlated to use them for extrapolation to the regions where no experimental information is available. Similar behavior has been observed in energy-energy correlations of nuclear reaction models (see Fig. 1 of Ref. [37]). From this figure we see that modifying model parameters affect the lightest as well as the heaviest nuclei. These strong correlations are at the basis of the strong predictive power of the HFB model.

B. Correlation between HFB model parameters

The 21 HFB parameters that have been varied are assumed to be independent. By definition, the initial backward MC covariance matrix therefore corresponds to the unitary matrix. However, as soon as experimental constraints are included in the forward method, correlations are introduced. These are illustrated in Fig. 6. The stronger the constraint (i.e., the lower χ_{crit}), the stronger the correlations. However, the level of

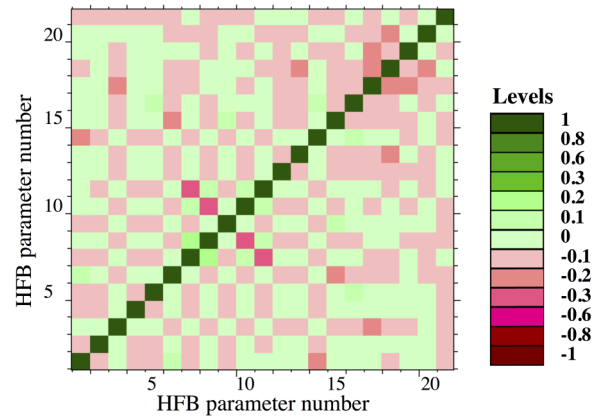

FIG. 6. (Color online) Color plot of the correlation matrix between the 21 model parameters (see upper x axis of Fig. 2 for the parameter labeling) considering the 1768 runs with $\sigma_{exp} < 0.6$ MeV.

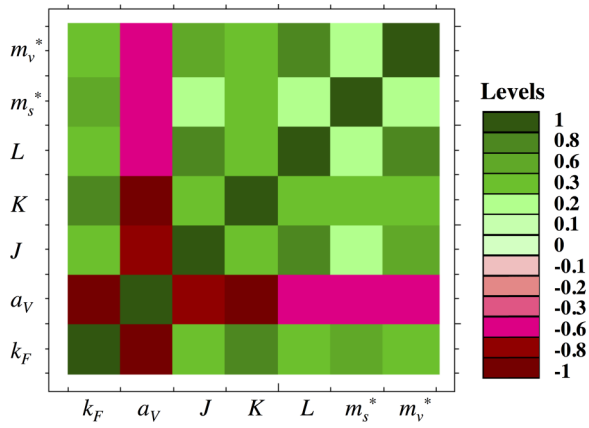

FIG. 7. (Color online) Color plot of the correlation matrix between the 7 INM model parameters (see Table I) considering the 11 013 runs with $\sigma_{\rm exp} < 0.8$ MeV.

correlation remains weak (typically smaller than ± 0.15). This can be understood through the large number of parameters and the various ways that can achieve the corresponding parameter change. The strongest correlations are found between the x_0 and x_1, x_0 and x_3, x_1 and x_4, x_3 and x_4, and anticorrelations between x_1 and x_3 and x_0 and x_4. The four pairing parameters f_q^π (parameter number 17 to 20) also present nonnegligible anticorrelations, in particular f_n^+ and f_n^- as well as f_n^+ and f_p^+. Note that the correlations between our HFB model parameters are globally found to be smaller than those obtained in Refs. [12,13]. This can partially be explained by the larger number of parameters in our framework, which implies that a given parameter change can be counterbalanced in more ways than if only a few parameters were varied.

C. Correlation between INM model parameters

Of particular interest are the correlations between the INM parameters. Only seven INM parameters have been considered here, as shown in Table I. The correlation matrix is shown in Fig. 7 in the case of the 11 013 runs with $\sigma_{\rm exp} < 0.8$ MeV. Very strong correlations exist among all the parameters, except maybe between M_s^* and J, L, or M_v^*. Part of these correlations is due to the model framework, another part is due to the constraint on the experimental masses. To illustrate this feature, we show in Fig. 8 the correlation plots between J and the other six INM parameters. Clearly, there exist no intrinsic model correlations between J and k_F, a_V, K, or M_s^*, but a strong correlation between J and L and a nonnegligible correlation between J and M_v^* is clearly inherent to our HFB framework. Similar results can be found in the correlation matrices of Refs. [12,13]. However, the constraint on experimental masses (red diamonds and blue open circles in Fig. 8) brings additional and significant correlations between these parameters, except between J and M_s^*, as already pointed out in Fig. 7.

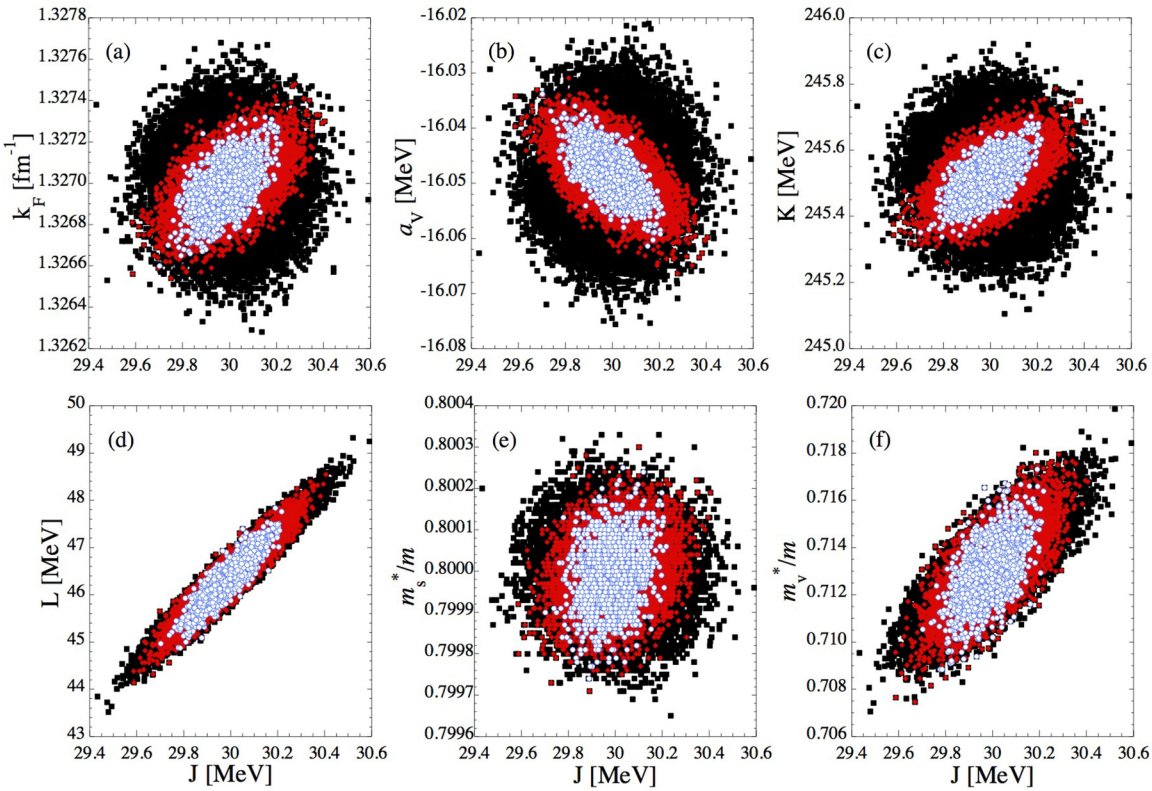

FIG. 8. (Color online) Correlation between the symmetry coefficient J and the six other INM properties considered in the present paper, i.e., (a) k_F, (b) a_V, (c) K, (d) L, (e) M_s^*, and (f) M_v^*. The black squares correspond to the 29 300 runs, the red diamonds to the 11 013 runs with $\sigma_{\rm exp} < 0.8$ MeV, and the blue open circles to the 1768 runs with $\sigma_{\rm exp} < 0.6$ MeV.

V. CONCLUSION

A variation of the BFMC approach has been applied to estimate the uncertainties on theoretical mass predictions associated with the HFB parameters in the vicinity of the HFB-24 local minimum. Making use of different weighting functions in the BFMC framework, the uncertainties associated with local changes of the HFB parameters are found to remain smaller than those associated with nonlocal changes as described by the 27 HFB mass models. It should be kept in mind that this result has been obtained assuming the deformation energy is not affected by local parameter changes. Even if larger uncertainties could not be excluded for strongly deformed nuclei, our results are exact for the spherical nuclei and in particular for those lying close to the neutron shell closures of particular interest for r-process applications. This result also highlights that differences between 27 HFB mass models are significant, but additional uncertainty is due to the parameter uncertainties for each model. The large number of degrees of freedom offered by the nonlocal changes also give rise to significantly different predictions of shell effects, pairing energies, and deformation transitions, while the present analysis restricts the changes in the vicinity of the local minimum and consequently does not allow for major changes.

ACKNOWLEDGMENT

S.G. acknowledges financial support from FNRS (Belgium).

[1] M. Bender, P.-H. Heenen, and P.-G. Reinhard, Rev. Mod. Phys. **75**, 121 (2003).
[2] D. Lunney, J. M. Pearson, and C. Thibault, Rev. Mod. Phys. **75**, 1021 (2003).
[3] M. Arnould, S. Goriely, and K. Takahashi, Phys. Rep. **450**, 97 (2007).
[4] J. M. Pearson, S. Goriely, and N. Chamel, Phys. Rev. C **83**, 065810 (2011).
[5] N. Chamel and P. Haensel, Living Rev. Relativity **11**, 10 (2008), available online at http://www.livingreviews.org/lrr-2008-10.
[6] E. Bauge *et al.*, Technical Report No. NEA/NSC/WPEC/DOC (2010)427, NEA/WPEC-Subgroup 24 (OECD, Nuclear Energy Agency, 2011).
[7] D. L. Smith, Technical Report No. ANL/NDM-159 (Argonne National Laboratory, Argonne, IL, 2004).
[8] D. Neudecker, R. Capote, and H. Leeb, Nucl. Instrum. & Meth. Phys. Res. A **723**, 163 (2013).
[9] R. Capote, D. L. Smith, and A. Trkov, EPJ Web of Conferences **8**, 04001 (2010).
[10] D. L. Smith, in *Proceedings of the 8th International Topical Meeting on Nuclear Applications and Utilizations of Accelerators*, *Pocatello, July 29–August 2* (American Nuclear Society, La Grange Park, IL, 2007), p. 736.
[11] R. Capote and D. L. Smith, Nucl. Data Sheets **109**, 2768 (2008).
[12] M. Kortelainen, T. Lesinski, J. Moré, W. Nazarewicz, J. Sarich, N. Schunck, M. V. Stoitsov, and S. Wild, Phys. Rev. C **82**, 024313 (2010).
[13] M. Kortelainen, J. McDonnell, W. Nazarewicz, P. G. Reinhard, J. Sarich, N. Schunck, M. V. Stoitsov, and S. M. Wild, Phys. Rev. C **85**, 024304 (2012).
[14] M. Samyn, S. Goriely, P.-H. Heenen, J. M. Pearson, and F. Tondeur, Nucl. Phys. A **700**, 142 (2002).
[15] S. Goriely, M. Samyn, P.-H. Heenen, J. M. Pearson, and F. Tondeur, Phys. Rev. C **66**, 024326 (2002).
[16] M. Samyn, S. Goriely, and J. M. Pearson, Nucl. Phys. A **725**, 69 (2003).
[17] S. Goriely, M. Samyn, M. Bender, and J. M. Pearson, Phys. Rev. C **68**, 054325 (2003).
[18] M. Samyn, S. Goriely, M. Bender, and J. M. Pearson, Phys. Rev. C **70**, 044309 (2004).
[19] S. Goriely, M. Samyn, J. M. Pearson, and M. Onsi, Nucl. Phys. A **750**, 425 (2005).
[20] S. Goriely, M. Samyn, and J. M. Pearson, Nucl. Phys. A **773**, 279 (2006).
[21] S. Goriely, M. Samyn, and J. M. Pearson, Phys. Rev. C **75**, 064312 (2007).
[22] S. Goriely and J. M. Pearson, Phys. Rev. C **77**, 031301 (2008).
[23] N. Chamel, S. Goriely, and J. M. Pearson, Nucl. Phys. A **812**, 72 (2008).
[24] S. Goriely, N. Chamel, and J. M. Pearson, Phys. Rev. Lett. **102**, 152503 (2009).
[25] N. Chamel, S. Goriely, and J. M. Pearson, Phys. Rev. C **80**, 065804 (2009).
[26] S. Goriely, N. Chamel, and J. M. Pearson, Phys. Rev. C **82**, 035804 (2010).
[27] S. Goriely, N. Chamel, and J. M. Pearson, Phys. Rev. C **88**, 024308 (2013).
[28] S. Goriely, N. Chamel, and J. M. Pearson, Phys. Rev. C **88**, 061302 (2013).
[29] G. Audi, M. Wang, A. H. Wapstra, F. G. Kondev, M. MacCormick, X. Xu, and B. Pfeiffer, Chinese Physics C **36**, 1287 (2012).
[30] Z. H. Li and H.-J. Schulze, Phys. Rev. C **78**, 028801 (2008).
[31] G. Colo, N. V. Giai, J. Meyer, K. Bennaceur, and P. Bonche, Phys. Rev. C **70**, 024307 (2004).
[32] M. B. Chadwick, T. Kawano, P. Talou, E. Bauge, S. Hilaire, P. Dossantos-Uzarralde, P. E. Garett, J. A. Becker, and R. O. Nelson, Nucl. Data Sheets **108**, 2742 (2007).
[33] E. Bauge, S. Hilaire, and P. Dossantos-Uzarralde, in *Proceedings of the International Conference on Nuclear Data for Science and Technology (ND2007)*, edited by O. Bersillon, F. Gunsing, E. Bauge, R. Jacqmin, and S. Leray (EDP Sciences, Les Ulis, 2008), p. 259.
[34] E. Bauge and P. Dossantos-Uzarralde, J. Korean Phys. Soc. **59**, 1218 (2011).
[35] R. Capote, D. L. Smith, A. Trkov, and M. Meghzifene, J. ASTM International **9**, 104115 (2012).
[36] P.-G. Reinhard and W. Nazarewicz, Phys. Rev. C **81**, 051303(R) (2010).
[37] A. Trkov, R. Capote, E. Sh. Soukhovitskii, L. C. Leal, M. Sin, I. Kodeli, and D. W. Muir, Nucl. Data Sheets **112**, 3098 (2011).